Formation of High-Stress Phase and Extrusion of Polyethylene due to Nanoconfinements during Ziegler−Natta Polymerization Inside Nanochannels

Sujith Nair, Prabhat Naredi, and Seong H. Kim*

Department of Chemical Engineering, The Pennsylvania State University, University Park, Pennsylvania 16802

Received: April 6, 2005

Polyethylene nanofibers were synthesized by heterogeneous Ziegler−Natta polymerization inside nanochannels of robust anodized aluminum oxide (AAO) membranes. The polymerization catalysts were chemisorbed at the inner wall of the nanochannels and monomers were provided through diffusion from the outside. Polyethylene is produced inside the nanochannels in the 10−20 μm region from the channel entrance. Polyethylene fibers were extruded from the nanochannels up to 3−5 μm during the polymerization. X-ray diffraction, differential scanning calorimetry, and Fourier transform infrared analyses indicated formation of a highly stressed crystalline structure although the polymerization was carried out without any external pressure or mechanical work. The highly stressed phase formation inside nanochannels and some degree of polyethylene nanofiber extrusion from nanochannels were attributed to catalytic production of excess amounts of polyethylene inside nanoconfined templates.

I. Introduction

Development of engineered nanomanufacturing processes is very important to utilize nanomaterials in more efficient ways.[1,2] One of the biggest challenges in this area is to accomplish simultaneous synthesis and alignment of one-dimensional nanomaterials. In nature, spiders weave webs by aligning silky fibers while they are producing fibers.[3] By doing so, these small creatures in nature do not face difficulties of grabbing and aligning tiny fibers out of a reservoir containing randomly oriented fibers. To achieve the simultaneous synthesis and alignment, one must be able to continuously synthesize and extrude nanomaterials from nanoscale reactors.

The prerequisites for simultaneous synthesis and extrusion of polymeric nanowires from the nanoscale reactor are continuous monomer supply into the reactor and application of enough forces to push out the produced polymers from the reactor. The monomer supply can be easily attained through diffusion. Even after the reactor is filled with polymers, monomer diffusion can occur through the polymer since the monomer molecules can readily be dissolved in the same kind of polymer.[4] The bigger challenge is how to apply high enough forces to push out the polymer from the nanoscale reactor. In atomic force microscopy studies, the typical adhesion force between polymers and inorganic surfaces such as silicon oxide is measured to be 1−10 nN for 20−30 nm diameter tips in ambient air or dry conditions.[5] This corresponds to 10^3−10^4 nN for 1 μm long polymer section in a 200 nm diameter channel. To generate an extrusion force comparable to this, a pressure gradient of ∼1 GPa should be applied across the nanoreactor structure. This is almost the same order of magnitude to, or slightly higher than, the yield stress of polyethylene.[6] However, applying this high pressure to only one side of nanoscale reactors such as mesoporous templates with macroscopic devices is practically not possible. This is the main reason that the templated synthesis approaches often rely on destruction of the templates for retrieval of nanomaterials, rather than extrusion.

One way of solving this problem is to generate the required stress (or pressure) inside the nanochannel to aid polymer extrusion. Consider the Ziegler−Natta polymerization which occurs spontaneously upon contact of monomers with the catalytic centers.[7−9] Since the chemical potential of polymers is larger than that of monomers in the vicinity of the catalytic sites, the polymerization does not stop simply because the headspace above the catalyst is filled with polymers. As long as monomers are available to the active catalytic sites by diffusion through the growing polymer layers, the polymerization continues producing excess amount of polymers.[9] This excess polymer production in a confined geometry causes increase of an internal stress that can eventually induce disintegration of the template structure. These examples are fragmentation of catalyst particles in olefin polymerization with Ziegler−Natta catalyst loaded inside microporous $MgCl_2$ supports and delamination of clay materials upon metallocene-catalyzed polymerization inside clay layers.[10−13]

This work explores the possibility of polymer extrusion driven by Ziegler−Natta polymerization inside nanotemplates which do not disintegrate upon growth of excess polymers. An anodized aluminum oxide (AAO) membrane was chosen as a test nanotemplate. Commercially available AAO membranes are composed of an array of ∼200 nm wide, ∼60 μm long nanochannels that are evenly distributed over the whole membrane surface. The symmetric arrangement of nanochannels and the high hardness of the aluminum oxide allow balanced distribution of the stress generated by growth of excess polymers inside nanochannels and prevent disintegration of the membrane structure. The aluminum oxide surface possesses a large number of hydroxyl (OH) groups to which the Ziegler−Natta catalyst titanium tetrachloride [$TiCl_4$] and cocatalyst triethylaluminum [$Al(C_2H_5)_3$] can be chemisorbed.

We studied catalytic production of polyethylene from gas-phase ethylene using Ziegler−Natta catalysts loaded in the inner walls of AAO nanochannels (Figure 1). The adhesion between the polymer and the nanochannel wall is very high in the absence of any solvent; thus, the polymer extrusion during gas-phase

* Corresponding author. E-mail: shkim@engr.psu.edu.

10.1021/jp051772q CCC: $30.25
Published on Web 06/08/2005

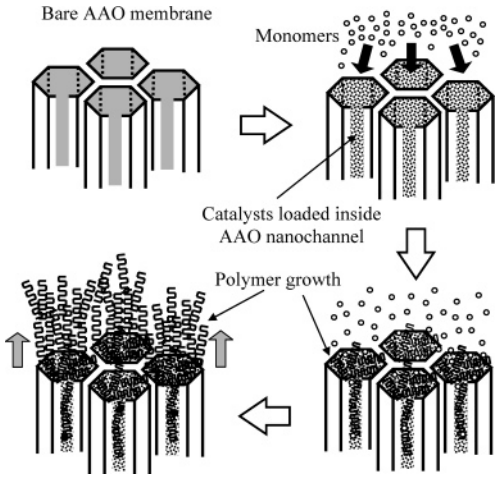

Figure 1. Schematics of the Ziegler−Natta ethylene polymerization processes in nanochannels of anodized aluminum oxide. (a) This illustrates the bare AAO nanochannel with section cut. (b) Ziegler−Natta catalysts loaded inside AAO nanochannels are exposed to monomers. (c) Polymerization occurs inside the nanochannels. The monomer molecules still diffuse through the polymer-filled nanochannels to the active catalytic sites. (d) The continued polymerization inside the nanochannel produces excess polymers that causes accumulation of stress inside the nanochannels and eventually pushes polymer chains out.

polymerization is much more difficult than extrusion during polymerization in solution.[14] The structural analysis of the produced polyethylene indicates that the polymer chains appear to be packed into an extremely highly stressed structure that resembles a high-pressure phase even though the reaction is carried out at near atmospheric pressure. Scanning electron microscopy reveals that some of the produced polymers are extruded out of the nanochannels with the dimension defined by the nanochannel diameter. The structure of polyethylene produced inside AAO nanochannels, the extrusion of the produced polyethylene, and the limitation of this approach are discussed in this paper.

II. Experimental Section

II.1. Materials. A commercially available AAO membrane (Whatman Anodisc 13) was used as a model nanochannel reactor. High-purity $TiCl_4$ and $Al(C_2H_5)_3$ were purchased and further purified with freeze−pump−thaw cycles after being connected to the gas line of the reactor system. A polymer-grade ethylene gas (99.95%) was used without further purification. A commercial high-density polyethylene (HDPE, molecular weight $\approx$ 125 000) was purchased and used for structural comparison with the polyethylene produced inside nanochannels.

II.2. Synthesis of Polyethylene in Nanochannels of AAO Membrane. The reaction chamber consisted of a high-pressure reaction cell attached to the preparation chamber of a VG ESCA system. In this setup, the sample can easily be loaded into and retrieved from the vacuum and transferred from one compartment to another without exposing it to air. A fresh AAO membrane was heated to 250 °C in the vacuum to eliminate physisorbed water inside the membrane. $TiCl_4$ was chemisorbed onto the inner and outer surfaces of the AAO membrane at 300 mTorr and then activated with $Al(C_2H_5)_3$ at ~60 mTorr in the high-pressure cell. Care was taken to avoid condensation of $Al(C_2H_5)_3$ liquid layers on the AAO membrane. Each gas was pumped out thoroughly before introduction of the next stream to avoid gas-phase reactions. The catalyst loading on the membrane was monitored with X-ray photoelectron spectroscopy (XPS) in the VG ESCA system and confirmed by comparing these data with the literature.[15−17] The homogeneous loading of the Ziegler−Natta catalyst was checked with ex-situ imaging XPS of the cross-section of the $TiCl_4$-loaded AAO membrane using Kratos Analytical Axis Ultra XPS. The catalytic sites at the outer surface of the membrane were removed by argon ion sputtering in the VG ESCA system. After argon sputtering, the AAO membrane sample was transferred to the high-pressure reaction cell and then exposed to 1000 Torr (~1.3 atm) of ethylene gas at room temperature. The polymerization time was varied from 1 to 12 h. But, the amount of polymer produced did not increase with the polymerization time in these conditions.

II.3. Characterization of the Polyethylene Produced. The produced polyethylene samples were characterized by Fourier transform infrared spectroscopy (FTIR), X-ray diffraction (XRD), scanning electron microscopy (SEM), differential scanning calorimetry (DSC), and gel permeation chromatography (GPC). All analyses, except GPC, were made without separating polymers from AAO membranes. In fact, the membrane worked as a support in FTIR, XRD, and SEM. FTIR analysis was done with Thermo-Nicolet 760. The FTIR spectrum was analyzed only in the 1200−4000 cm^{-1} range because aluminum oxide is not transparent to IR below 1200 cm^{-1}. For temperature dependence FTIR measurements, a home-built AAO membrane heater was used. In the case of a reference sample, a thin film was prepared and sandwiched between AAO membranes, heated above the melting temperature, and cooled to room temperature while collecting FTIR spectra in real time. XRD was performed using Philips X'Pert MPD. The broad background scattering due to amorphous AAO was subtracted from the XRD spectrum of the polyethylene sample produced inside the AAO membrane. The top and cross-section topography of AAO membrane samples before and after polymerization were obtained with SEM (JEOL Philips XL-20). For SEM imaging, a thin layer of gold was coated on the samples to prevent charging. Thermal analysis was carried out with DSC (QA 1000, Texas Instruments) at a heating rate of 10 °C/min and a cooling rate of 5 °C/min. For molecular weight analysis, polymers were extruded with hot trichlorobenzene from ~15 polymerization runs and analyzed with GPC at the DuPont Analytical Services Center.

III. Results

III.1. Extrusion of Polyethylene from Nanochannels during Polymerization. Polyethylene was reproducibly produced with the process described in Section II.2. The XPS analysis after polymerization showed only a C1s peak and no discernible peaks of titanium species or aluminum oxide species from the substrate. The balance band spectrum showed two peaks at 14.5 and 20 eV, which are characteristic to polyethylene, indicating the AAO membrane is fully covered with polyethylene.[9] This is confirmed with SEM imaging. The top image of the AAO membranes after polymerization (Figure 2b) clearly shows that the surface is fully packed with about 200−400 nm circular polymeric species. The diameter of these individual circular features is comparable with or slightly larger than the nanochannel diameter of the bare AAO membrane (Figure 2a).

The cross-section images of the AAO membrane fractured after polymerization, shown in Figure 2c, provides more information on the polymerization/extrusion process. The most important feature of this cross-section image is that bundles of polyethylene nanofibers can be seen above the membrane. The length of polyethylene fibers above the AAO membrane varies run to run; it is typically in the range of 3−5 μm. Some fiber

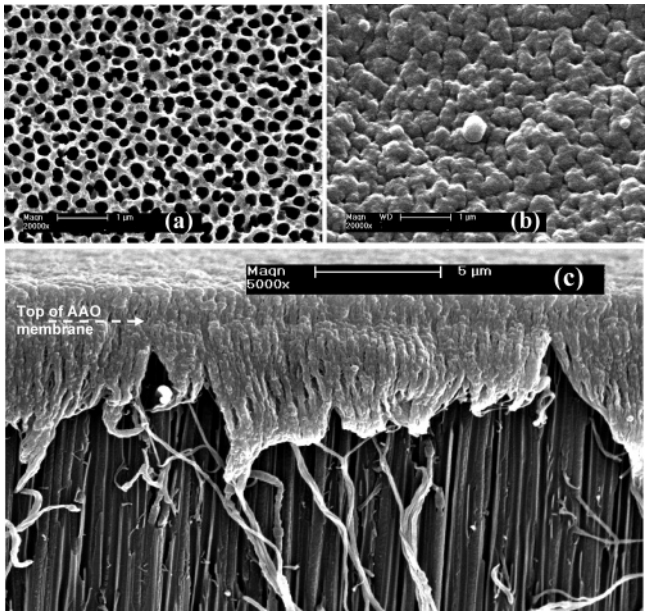

Figure 2. SEM image of (a) the top surface of the bare AAO membrane, (b) the top surface of the polyethylene layer produced by Ziegler−Natta polymerization within AAO nanochannels, and (c) the cross-section of the AAO membrane after ethylene polymerization. The dotted line in c indicates the position of the AAO membrane top surface. (Scale bars = 1 μm in a and b and 5 μm in c).

bundles originally grown on the opposite surface of the fractured pieces are separated from the membrane and attached to the imaged section. These bundles fall down and cover the top edge of the AAO membrane fracture surface. The diameters of polyethylene fibers are very close to the nanochannel diameter. The surface of all the fibers outside the membrane is corrugated. This kind of corrugated surface texture is typically observed for macroscopic polymeric fibers produced by extrusion;[18,19] the nanoscale extrusion and corrugation have not been reported in the literature. Some degree of corrugated surface texture can also be seen for fibers still present inside nanochannels and exposed upon cracking of the membrane. Individual fibers seen in this image clearly indicate that the polyethylene nanofiber bundles are made with diameters defined by the nanochannel diameters, and some amount of these nanofibers are extruded out of the nanochannels during the Ziegler−Natta polymerization inside AAO nanochannels.

Another important feature observed in the cross-section SEM analysis is the distribution of polyethylene inside the AAO nanochannels. As shown in Figure 2c, the top part of the AAO nanochannels exposed to monomers for polymerization is completely filled with polyethylene. Some polyethylene fibers are partially pulled out of nanochannels during the fracture. The polyethylene fibers in the empty channels of this image must be attached to the opposite side of the fracture surface. In contrast, the bottom part of the nanochannels is not fully filled with polyethylene [see Supporting Information]. Instead, a large number of polymer dots and short fibers are observed on the inner walls. The diameter of these short fibers are much smaller than the nanochannel diameter, and most of them appear to be attached to the fracture edge of the nanochannel wall, suggesting that the tiny fibers are produced by pulling polymer dots at the fracture interface when the AAO membrane is fractured. In the middle, a clear boundary between the completely filled top region and the partially filled bottom region is observed. The length of AAO nanochannels fully filled with polymers is about 15−20 μm from the top.

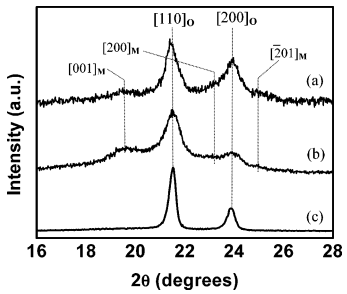

Figure 3. XRD pattern of (a) polyethylene produced inside AAO nanochannels, (b) polyethylene produced on flat surfaces, and (c) HDPE. In a, the broad background contribution from the amorphous aluminum oxide is subtracted for easy comparison of polyethylene features. Subscripts O and M after the Miller indices indicate orthorhombic and monoclinic phases, respectively.

The reason for incomplete filling with polymers in the lower part of the nanochannel cannot be due to inhomogeneous distribution of the Ziegler−Natta polymerization catalyst along the channel length. In the titanium ion distribution image obtained with spatially resolved XPS analysis [shown in Supporting Information], the titanium ions are found to be evenly distributed along the entire length of the nanochannels (60 μm). The limited growth of polymer dots in the bottom section of the nanochannels must be related to mass transport of ethylene monomers through the region filled with polyethylene. More details will be discussed in the later section along with generation of the extrusion force.

III.2. Structural Analysis of Polyethylene Produced Inside AAO Nanochannels. The structure of polyethylene produced inside AAO nanochannels (hereafter, PE-AAO) are analyzed with XRD and compared with those of a melt-pressed sample of a reference high-density polyethylene (HDPE) and a polyethylene film produced on flat alumina supports with the same Ziegler−Natta chemistry in the same reaction cell (PE-flat). On the flat support, the Ziegler−Natta polymerization catalyst loading occurs basically the same way on the AAO membrane surface—through chemisorption at surface OH groups. Figure 3 shows XRD peaks in the 2θ region of 15−28° of PE-AAO, PE-flat, and HDPE. The two dominant peaks at 21.5 and 23.8° that can be seen for all three samples correspond to diffraction peaks of the [110] and [200] planes, respectively, of the orthorhombic structure, which is the thermodynamically most stable phase at ambient conditions.[20,21] The *a* and *b* lattice spacing calculated from these two diffraction peaks are within experimental errors from the theoretical values of the orthorhombic phase. The *c* axis dimension cannot be determined because [011], [111], and [201] peaks at 39.8, 41.7, and 43.1°, respectively, are not observed due to weak intensities of these peaks for thin PE-AAO and PE-flat samples. Broad peaks at 19.5, 23.1, and 25.1° correspond to the [001], [200], and [201] planes, respectively, of the monoclinic phase. This metastable phase is frequently observed in catalytically produced, unannealed polyethylene samples or mechanically strained polyethylene samples.[22−24] A broad, low-intensity background is due to the presence of the amorphous phase in the unannealed polyethylene samples. The crystallinity of these samples is calculated from deconvolution of XRD peaks shown in Figure 3 and summarized in Table 1. Large amounts of monoclinic phase for the unannealed PE-AAO and PE-flat are consistent with the literature.[25]

The most important difference of the XRD patterns of PE-AAO from those of HDPE and PE-flat is the relative intensity ratio of the two orthorhombic phase peaks $-I_{[200]}/I_{[110]}$.

TABLE 1: Comparison of Crystallinity Values for PE-AAO, PE-Flat, and HDPE Samples

sample	orthorhombic phase (%)	monoclinic phase (%)	total crystallinity (%)
PE-AAO as-produced	55	22	72
PE-flat as-produced	51	28	79
HDPE	88	not present	88
PE-AAO melt/cooled	88	not present	88
PE-flat melt/cooled	89	not present	89

This ratio is 0.5−0.55 for PE-AAO and 0.3−0.35 for HDPE and PE-flat. This clearly indicates that although their unit cell dimensions are not significantly different, the polymer chains in the PE-AAO sample are packed somewhat differently than those in the HDPE and PE-flat samples. We will call this a "nanoconfinement-induced" phase to distinguish it from the normal thermodynamically preferable phase. The origin of the nanoconfinement-induced phase will be discussed in the next section.

Vibrational spectroscopic analysis provides further information on the nanoconfinement-induced phase. All samples show only four peaks characteristic to polyethylene—two peaks at 2920 and 2850 cm^{-1} of asymmetric and symmetric C−H stretching vibrations and two peaks at 1474 and 1464 cm^{-1} of CH_2 bending vibrations. Figure 4 compares the CH_2 bending vibration region of FTIR spectra of three samples shown in Figure 3. It can be clearly seen that the I_{1474}/I_{1464} ratio is significantly different for all three samples. The PE-AAO sample shows the highest I_{1474}/I_{1464} value of ∼2.0, the PE-flat sample has ∼1.2, and the HDPE sample gives about 0.95. In the case of HDPE, the splitting of the CH_2 bending vibration into two peaks is due to the interchain interactions in the orthorhombic crystal structure.[26] The theoretical ratio for 100% crystalline polyethylene is ∼1.233.[26] The crystallinity value calculated for HDPE from this FTIR result is ∼88.3%,[27] which is consistent with that calculated from XRD. In the case of PE-flat, the additional enhancement of the 1474 cm^{-1} peak intensity giving rise to the I_{1474}/I_{1464} ratio higher than 1.1 is due to the presence of the monoclinic phase as indicated by XRD. The monoclinic phase has a single peak at 1475 cm^{-1}.[25]

The origin of the high I_{1474}/I_{1464} ratio for PE-AAO cannot be attributed to the presence of the monoclinic phase since XRD shows that the amount of monoclinic phase in the PE-AAO is smaller than that in the PE-flat. One can speculate a preferential orientation of the orthorhombic crystalline domain inside AAO nanochannels. We have checked this with a polarization dependence of FTIR spectra following the method reported by Huang et al.[27] The I_{1474}/I_{1464} ratio does not show any polarization angle dependence [results shown in Supporting Information]. Therefore, the preferential orientation of the orthorhombic phase can be ruled out. The unusually high I_{1474}/I_{1464} ratio must be directly related to the formation of the nanoconfinement-induced phase.

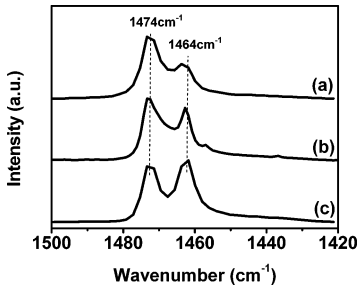

Figure 4. CH_2 bending vibration region of FTIR spectra of (a) polyethylene produced inside AAO nanochannels, (b) polyethylene produced on flat surfaces, and (c) HDPE.

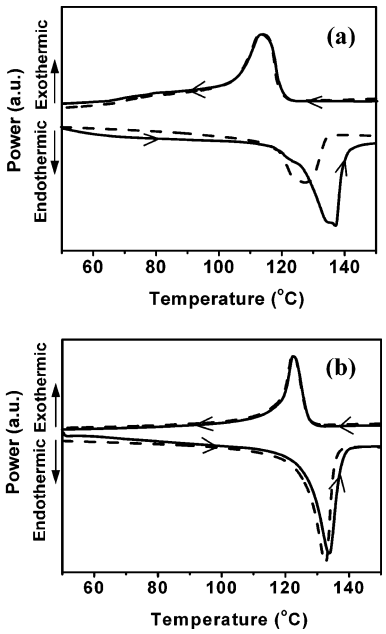

Figure 5. DSC thermograms of (a) polyethylene produced inside AAO nanochannels and (b) polyethylene produced on flat surfaces. The solid lines are data from the first heating and cooling cycle, and the dashed lines are data from the second heating and cooling cycle.

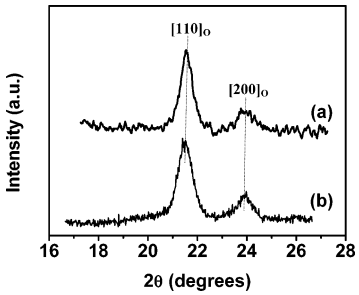

Figure 6. XRD pattern of melt and recrystallized samples of (a) polyethylene produced inside AAO nanochannels and (b) polyethylene produced on flat surfaces. The samples were heated to 150 °C for 30 min and then cooled in dry nitrogen.

The melting behavior of PE-AAO observed in DSC is very interesting (Figure 5). While PE-flat displays the typical first-order phase transition shape centered at ∼133 °C, PE-AAO reveals a broader melting peak with a sharp drop at ∼139 °C. Upon recrystallization, PE-flat and HDPE show the typical crystallization behavior of polymer samples, but PE-AAO shows a broader transition. In the second heating and cooling cycle, PE-flat and HDPE show no change from the first heating and cooling cycle; in contrast, PE-AAO melts at a lower temperature ($\Delta T_m \sim 10$ °C) in the second heating. For all three samples, the second recrystallization profile exactly follows the first recrystallization profile. The lower melting temperature of PE-AAO in the second heating cannot be attributed to polymer separation from the AAO membrane. SEM imaging of the melted and cooled PE-AAO sample shows that polymers are still present inside AAO nanochannels. Therefore, the decrease of the polymer melting temperature after the first heating cycle implies that the nanoconfinement-induced phase is destroyed during the heat treatment.

The disappearance of the nanoconfinement-induced phase and the monoclinic phase upon annealing is confirmed with XRD. Figure 6 compares the XRD data of PE-AAO and PE-flat samples after heating to ∼150 °C and then cooling to room temperature. Both samples show the orthorhombic structure with

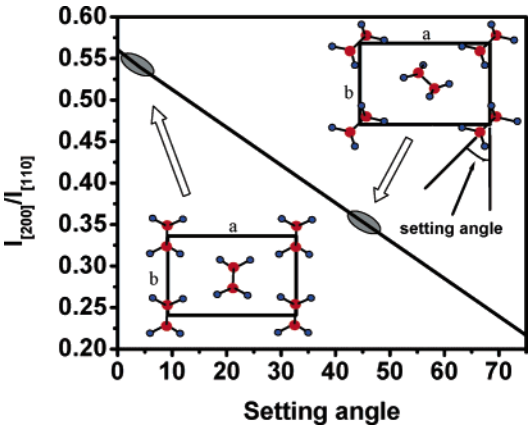

Figure 7. Simulated prediction of the $I_{[200]}/I_{[110]}$ ratio as a function of setting angle. The setting angle is defined as the angle between the *b* axis of the orthorhombic phase unit cell and the CH_2-CH_2 molecular axis of the polyethylene chain aligned along the *c* axis. Also shown are the schematics of the molecular arrangements at two different setting angles.

a very high crystallinity. These results indicate that the nanoconfinement-induced phase is not thermodynamically stable at ambient conditions and can be removed by simple thermal annealing.

The molecular weight analysis of PE-AAO and PE-flat shows that both samples have a very broad molecular weight distribution. The number-averaged (M_n) and weight-averaged (M_w) molecular weights are 6188 and 292 804, respectively, for PE-AAO, giving rise to a polydispersity (M_w/M_n) of ~47. The M_n and M_w for PE-flat are 36 344 and 1255 940, respectively, giving rise to a polydispersity of ~35. The broad polydispersity for polymers produced with Zigler−Natta catalysts loaded on alumina surfaces indicates that the catalyst sites have a wide range of polymerization activities. It may also be related to monomer diffusion through the polymer layer growing from the catalyst sites. The lower molecular weights and broader distribution for PE-AAO, compared to those of PE-flat, also seem to be related to the monomer diffusion. Since there is no lateral diffusion across the nanochannel walls, the monomer supply to the catalytic sites inside nanochannels filled with polymers would be more difficult than the monomer supply to those on a flat substrate surface.

IV. Discussion

IV.1. Nanoconfinement Effects on Polyethylene Packing in PE-AAO. From structural and thermal analyses, it is clear that the Ziegler−Natta polymerization of ethylene inside AAO nanochannels produces polyethylene that has a molecular packing structure different from those produced by thermal treatments or without nanoconfinements. The nanoconfinement during the polymerization gives the enhanced $I_{[200]}/I_{[110]}$ ratio in XRD and the enhanced I_{1474}/I_{1464} ratio in FTIR. To get more detailed physical insights into the nanoconfinement effects, the setting angle ($\theta_{setting}$) between the C−C bond of polyethylene and the *b* axis of the orthorhombic unit cell is analyzed with XRD data shown in Figure 3. The $I_{[200]}/I_{[110]}$ ratio for different setting angles is simulated using an X-ray crystallographic simulation software.[28] The simulation result is shown in Figure 7. This simulation is done by rotating the CH_2-CH_2 axis in the *ab* plane of the unit cell with the center of the CH_2-CH_2 group fixed at its original position of the orthorhombic structure.[29,30] The simulation clearly indicates that the $I_{[200]}/I_{[110]}$ ratio increases in proportion to the decrease of the setting angle. From this simulation data, one can find that the $I_{[200]}/I_{[110]}$ ratio of 0.3−0.35 observed for PE-flat and HDPE corresponds to the setting angle of ~46°, which is consistent with the polyethylene chain packing in the normal orthorhombic phase.[29,30] In this structure, the CH_2-CH_2 groups are arranged in a herringbone structure. The $I_{[200]}/I_{[110]}$ ratio of 0.5−0.55 observed for PE-AAO indicates that the CH_2-CH_2 groups are almost parallel to the *b* axis when polyethylene is produced catalytically inside nanochannels. These results clearly imply that the nanoconfinement-induced phase in PE-AAO has a chain packing structure that is not observed in regular HDPE and PE-flat.

The observation of a low setting angle in the polyethylene unit cell has been reported in the literature. When the pressure applied to polyethylene during the recrystallization is increased from 1 to 6000 bar, the setting angle decreases gradually from 48 to 44°.[31] There are a number of reports on formation of a hexagonal phase at high pressures (>3000 bar) and high temperatures (>235 °C).[32−34] The hexagonal phase can be induced if the setting angle in the orthorhombic phase is reduced to zero or completely randomized and the *a* and *b* axis dimensions of the orthorhombic phase are slightly altered such that the center of CH_2-CH_2 group is located at the 3-fold symmetry positions. Since the *a* and *b* axis dimensions of the nanoconfinement-induced phase of PE-AAO are still close to those of the orthorhombic phase, it cannot be said that this phase is hexagonal. It might rather be related to an intermediate structure occurring in transition from the normal orthorhombic phase in ambient conditions to the hexagonal phase formed at high pressures and temperatures.

Other supporting evidence of the low-setting-angle structure is the melting behavior of the PE-AAO sample. The DSC analysis shows that PE-AAO melts at a slightly higher temperature ($\Delta T_m \sim 10$ °C) in the first heating compared to the second heating. This is consistent with the characteristic behavior of the high-pressure phase with low setting angles reported in the literature.[31,35−38] The melting temperature change cannot be explained with the low and broad molecular weight distribution for PE-AAO because the molecular weight does not vary during the DSC analysis in inert environment. The broader melting and recrystallization behavior for PE-AAO, compared to PE-flat, might be related to the broader molecular weight distribution or interactions with aluminum oxide surfaces.

IV.2. Extrusion Driving Force. What is remarkable in this study is that the low-setting-angle structure pertaining to the high-stress phase is obtained during the polymerization only at 1.3 atm. The exact stress generated inside the AAO nanochannels during the Ziegler−Natta polymerization of ethylene cannot be measured in our experimental conditions. However, a first-order approximation can be made on the basis of the literature information. If the setting-angle dependence on the applied pressure reported in the literature is extrapolated to the near-zero setting angle,[31] it predicts that a pressure (stress) higher than 1 GPa is needed to get a near-zero setting-angle structure. Though this is a first-order approximation, it is interesting that this simple prediction finds the stress estimated to be required for extrusion of polymers from nanochannels.

The high internal stress buildup is believed to originate from the resistance to polymer flow due to strong adhesion between the polymer and the nanochannel wall. As discussed before, simple van der Waals interactions can generate enormous adhesion forces in the nanoscale. The chemical bonds between chemisorbed catalysts and polymer chains will exert additional resistance against slipping polymers at the polymer/nanochannel wall interface. Therefore, the production of excess polymers

due to favorable thermodynamic driving forces does not guarantee immediate extrusion of polymer out of nanochannels. Instead, it first causes buildup of a high stress inside the nanochannel. When the stress inside nanochannels becomes high enough to overcome polymer−surface adhesion or yield stress of the polymer, the polymeric nanowire extrusion is finally occurring. This extrusion process cannot be observed if the nanotemplate is not strong enough to sustain the high stress. These are the cases of microporous $MgCl_2$ and clays.[10−13]

We cannot exactly determine the effective depth in which the extrusion process occurs. It is very likely to be limited to the region near the nanochannel exit. The polymers produced deep inside may not be able to come out in any circumstances because the accumulated adhesion force is so large. The polymers located beyond the possible extrusion depth will retain the high-stress phase even after completion of polymerization. Since these polymers deep inside nanochannels cannot move easily, the stress built-up during the polymerization cannot be released until enough thermal energy is provided for polymer chain relaxation or melting.

IV.3. Monomer Transport along the Nanochannel. Another important observation of this study is that polymers fill only the top 15−20 μm portion of the nanochannels, although the catalysts are coated over the entire 60 μm long channel. The region deeper than 15−20 μm contains only small polymer dots at the wall. This might be related to the effective diffusion length of ethylene monomer through polyethylene-filled inside nanochannels. The small polymer dots in the deeper region appear to be produced from the monomer gas that is supplied before the channel entrance is filled with the produced polymer. Once the channel entrance is fully filled with the polymer, the monomer supply into the deeper region is solely through diffusion. In our experiments, we cannot determine if (a) the maximum diffusion distance of monomer through the polymer fiber inside the nanochannel is only 15−20 μm or (b) the monomer can diffuse a longer distance but the catalysts are already deactivated by the time the monomer diffusion and polymer growth have reached that distance.

IV.4. Perspective. In most templated synthesis approaches,[39,40] one-dimensional nanomaterials are produced inside the templates, released into a solution, and recaptured onto a desired target substrate.[41,42] The recapture of a large number of these released nanomaterials with controlled alignments is extremely difficult due to the lack of enough enthalpy gain that can compensate for the large decrease of entropy upon transition from the randomly dispersed state in solution to the highly ordered state on substrate surfaces. This difficulty may be avoided if one can synthesize and extrude nanomaterials and transfer them directly to the target substrate while they are produced from an ordered array of nanoscale reactors.

Our original interest is to see if the macroscopic length of polymeric nanowire arrays can be produced in this way. But that does not seem to be possible with the Ziegler−Natta catalyst system used in this study. The maximum extrusion length does not exceed 10 μm from 200 nm diameter channels. This might be related to the catalyst deactivation. Although its activity is known to be extremely high, the lifetime of the Ziegler−Natta polymerization catalyst is limited due to deactivation.[12] Because of this, extrusion of polyethylene nanofibers using the Ziegler−Natta catalyst could not be sustained for an extended period of time to make fibers long enough for transfer onto a collector substrate. If one develops a polymerization catalyst with a high activity and a long lifetime, this approach might be able to produce arrays of macroscopic length polymeric nanowires that are long enough for transfer onto a substrate.

Similar concepts of polymeric nanowire production using nanostructured templates have been reported in previous literature.[14,43] In these studies, mesoporous silica powders dispersed in toluene solution were used as templates and polymerization of ethylene were carried out with metallocene catalysts in toluene solvent. The presence of solvent alleviates the polymer adhesion to the template wall and makes extrusion easier, but randomly dispersed fine template particles in solution produced an entangled mass of polymer fibers, rather than aligned nanofibers over a large area. In our approach, the aligned polyethylene nanofibers are attained and extruded over the entire surface of the AAO membrane, ~1 cm^2 area, without the aid of any external solvent. To the best of our knowledge, there has been no report in the literature on polymer extrusion from nanotemplates in the absence of any solvent and external work.

V. Conclusions

Continuous catalytic polymerization within mechanically strong nanotemplates results in formation of a high-stress crystalline structure and some degree of stress-induced extrusion of polymeric nanofibers. The Ziegler−Natta polymerization inside anodized aluminum oxide nanochannels with an average diameter of ~200 nm produces an excess amount of polymers. Since the adhesion of these polymer chains to the nanochannel walls is so strong, the excess polymers do not readily flow out of the nanochannel. Instead, they are packed in a highly stressed structure. The high-stress phase formation is supported by the high $I_{[200]}/I_{[110]}$ ratio in XRD, the high I_{1474}/I_{1464} ratio in FTIR, and the high melting temperature in DSC. The accumulation of stress due to excess polymer production eventually enables polymer extrusion out of nanochannels. The nanochannel diameter controls the diameter of the extruded polymeric nanowires. The high-stress crystalline structure is readily destroyed upon melting and not reproduced upon cooling the polymer melt inside the nanochannels.

Acknowledgment. This work is financially supported by National Science Foundation (Grant No. DMI-0210229).

Supporting Information Available: Imaging XPS data of titanium distribution across the AAO membrane cross-section, SEM images of different locations along the AAO nanochannels after Ziegler−Natta polymerization, SEM images of polymer fibers inside AAO nanochannels after a melting and cooling cycle, polarization-dependent FTIR data, and GPC analysis data of PE-AAO and PE-flat (PDF). This material is available free of charge via the Internet at http://pubs.acs.org.

References and Notes

(1) Collins, P. G.; Zettl, A.; Bando, H.; Thess, A.; Smalley, R. E. *Science* **1997**, *278*, 100.
(2) Steinhart, M.; Wendorff, J. H.; Greiner, A.; Wehrspohn, R. B.; Nielsch, K.; Schilling, J.; Choi, J.; Gosele, U. *Science* **2002**, *296*, 1997.
(3) Vollrath, F.; Knight, P. D. *Nature* **2001**, *410*, 541.
(4) Laso, M.; Jimeno, N.; Muller, M. *Polym. React. Eng.* **2003**, *11*, 1.
(5) *Microstructure and Microtribology of Polymer Surfaces*; Tsukruk, V. V., Wahl, K. J., Eds.; ACS Symposium Series 741; American Chemical Society: Washington, DC, 1999.
(6) Brooks, N. W.; Ghazali, M.; Duckett, R. A.; Unwin, A. P.; Ward, I. M. *Polymer* **1999**, *40*, 821.
(7) Hamba, M.; Han-Adebekun, G. C.; Ray, W. H. *J. Polym. Sci., Part A: Polym. Chem.* **1997**, *35*, 2063.
(8) Han-Adebekun, G. C.; Hamba, M.; Ray, W. H. *J. Polym. Sci., Part A: Polym. Chem.* **1997**, *35*, 2075.
(9) Kim, S. H.; Somorjai, G. A. *Catal. Lett.* **2000**, *68*, 7.
(10) Ruddick, V.; Badyal, J. P. S. *J. Phys. Chem. B* **1997**, *101*, 1791.

(11) Francois, H.; Philippe, D.; Robert, J.; Philippe, T.; Garcia, M. M. *J. Appl. Polym. Sci.* **1997**, *64*, 423.
(12) Yang, F.; Zhang, X.; Zhao, H.; Chen, B.; Huang, B.; Feng, Z. *J. Appl. Polym. Sci.* **2003**, *89*, 3680.
(13) Gopakumar, T. G.; Lee, J. A.; Kontopoulou, M.; Parent, J. S. *Polymer* **2002**, *43*, 5483.
(14) Kageyama, K.; Tamazawa, J.; Aida, T. *Science* **1999**, *285*, 2113.
(15) Kim, S. H.; Somorjai, G. A. *J. Phys. Chem. B* **2001**, *105*, 3922.
(16) Kim, S. H.; Somorjai, G. A. *J. Phys. Chem. B* **2000**, *104*, 5519.
(17) Kim, S. H.; Somorjai, G. A. *J. Phys. Chem. B* **2002**, *106*, 1386.
(18) Denn, M. M. *Annu. Rev. Fluid. Mech.* **2001**, 33, 265.
(19) Migler, K. B.; Son, Y.; Flynn, K. *J. Rheol.* **2002**, *46*, 383.
(20) Joo, Y. L.; Han, O. H.; Lee, H.-K.; Song, J. K. *Polymer* **2000**, *41*, 1355.
(21) Baker, A. M. E.; Windle, A. H. *Polymer* **2001**, *42*, 667.
(22) Russell, K. E.; Hunter, B. K.; Heyding, R. D. *Polymer* **1997**, *38*, 1409.
(23) Bartczak, Z.; Galeski, A.; Argon, A. S.; Cohen, R. E. *Polymer* **1996**, *37*, 2113.
(24) Vickers, M. E.; Fischer, H. *Polymer* **1995**, *36*, 2667.
(25) Seshadri, K.; Atre, V. S.; Tao, Y.-T.; Lee, M.-T.; Allara, D. L. *J. Am. Chem. Soc.* **1997**, *119*, 4698.
(26) Abbate, S.; Gussoni, M.; Zerbi, G. *J. Chem. Phys.* **1979**, *70*, 3577.
(27) Huang, J. B.; Hong, J. W.; Urban, M. W. *Polymer* **1992**, *33*, 5173.
(28) *Powder Cell*, V.13; Federal Institute for Material Research and Testing Laboratory: Berlin, Germany.
(29) Busing, W. R. *Macromolecules* **1990**, *23*, 4608.
(30) Kavesh, S.; Schultz, J. M. *J. Polym. Sci., Part A-2* **1970**, *8*, 243.
(31) Phillips, P. J.; Tseng, H. T. *Polymer* **1985**, *26*, 650.
(32) Bassett, D. C.; Block, S.; Piermarini, G. J. *J. Appl. Phys.* **1974**, *45*, 4146.
(33) Bassett, D. C. *High Temp.−High Pressures* **1977**, *9*, 553.
(34) Tashiro, K.; Sasaki, S.; Kobayashi, M. *Macromolecules* **1996**, *29*, 7460.
(35) Maxwell, A. S.; Unwin, A. P.; Ward, I. M.; El Maaty, M. I. Abo; Shahin, M. M.; Olley, R. H.; Bassett, D. C. *J. Mater. Sci.* **1997**, *32*, 567.
(36) Munehisa, Y.; Shinsuke, T.; Masashi, Y. *J. Polym. Sci. Part B: Polym. Phys.* **1997**, *35*, 535.
(37) Kuwabara, K.; Horii, F. *Macromolecules* **1999**, *32*, 5600.
(38) Kazmierczak, T.; Galeski, A. *J. App. Polym. Sci.* **2002**, *86*, 1337.
(39) Martin, B. R.; Dermody, D. J.; Reiss, B. D.; Fang, M.; Lyon, L. A.; Natan, M. J.; Mallouk, T. E. *Adv. Mater*. **1999**, *11*, 1021.
(40) Wu, C. G.; Bein, T. *Science* **1994**, *264*, 1757.
(41) Whang, D.; Jin, S.; Lieber, C. M. *Jpn. J. Appl. Phys.* **2004**, *43*, 4465.
(42) Smith, P. A.; Nordquist, C. D.; Jackson, T. N.; Mayer, T. S.; Martin, B. R.; Mbindyo, J.; Mallouk, T. E. *Appl. Phys. Lett.* **2000**, *77*, 1399.
(43) Ye, Z.; Zhu, S.; Wang, W.-J.; Alsyouri, H.; Lin, Y. S. *J. Polym. Sci., Part B: Polym. Phys.* **2003**, *41*, 2433.